Engineering Fracture Mechanics 268 (2022) 108493

Contents lists available at ScienceDirect

Engineering Fracture Mechanics

journal homepage: www.elsevier.com/locate/engfracmech

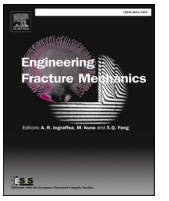

Experimental evaluation of cohesive laws components of mixed-mode I + II fracture characterization of cortical bone

Fábio Pereira [a,*], José Morais [a], José Xavier [b], N. Dourado [c], M.F.S.F. de Moura [d]

[a] CITAB, School of Science and Technology, University of Trás-os-Montes e Alto Douro, Vila Real 5001-801, Portugal
[b] UNIDEMI, Department of Mechanical and Industrial Engineering, NOVA School of Science and Technology, NOVA University Lisbon, 2829-516 Caparica, Portugal
[c] CMEMS-UMinho, Departamento de Engenharia Mecânica, Universidade do Minho, Campus de Azurém, Guimarães 4804-533, Portugal
[d] Faculdade de Engenharia da Universidade do Porto, Departamento de Engenharia Mecânica e Gestão Industrial, Rua Dr. Roberto Frias, 4200-465 Porto, Portugal

ARTICLE INFO

Keywords:
Cortical bone
Fracture characterization
Mixed-mode I+II loading
Cohesive laws
Digital image correlation

ABSTRACT

Mixed-mode I + II fracture characterization of cortical bone tissue is addressed in this work. The mixed-mode bending test was used to impose different mode ratios. An equivalent crack length data reduction method was considered to obtain the strain energy release rate components. Crack opening and shear displacements were measured by means of digital image correlation. These quantities were then integrated to propose a direct evaluation of cohesive laws. The components of the cohesive laws for each mixed-mode loading were obtained by the uncoupled and Högberg's methods. The later provided consistent evolution of strain energy release rate and peak stresses components in function of mode-ratio, revealing its appropriateness regarding the fracture characterization of cortical bone under mixed-mode I + II loading.

1. Introduction

Bone fractures are currently a relevant public health concern, due to increase of elderly population. They result in morbidity and mortality with relevant economic and social impacts. In this context, fracture characterization of bone is a vital research topic with significant influence on public health, which justifies its social-economic relevance. The large majority of the studies available in literature address pure mode I loading [1–6], and some works deal with mode II loading [1,7–9]. However, under general loading, fracture involves concurrently mode I and II (mixed-mode I + II). The non-symmetric geometry and bone irregular shape, associated with its marked anisotropy also contributes to fractures under mixed-mode I + II loading. Therefore, fracture analysis of cortical bone tissue under mixed-mode I + II loading can be viewed as relevant and emerging research topic. Few works describing mixed-mode I + II testing methodologies can be found in literature. George and Vashishth [10] studied the combined effect of axial and torsional fatigue/fracture loading considering cylindrical specimens to produce previously reported *in vivo* shear/normal stress ratios. Zimmermann et al., [8,9] used the asymmetric four-point bending test, which allows different combination of shear force and bending moment acting at the crack tip, providing fracture characterization under different mixed-mode I + II loading. Olvera et al. [11] employed the double cleavage drilled compression test in the context of mixed-mode I + II fracture characterization of cortical bone

* Corresponding author.
E-mail addresses: famp@utad.pt (F. Pereira), jmorais@utad.pt (J. Morais), jmc.xavier@fct.unl.pt (J. Xavier), nunodourado@dem.uminho.pt (N. Dourado), mfmoura@fe.up.pt (M.F.S.F. de Moura).

https://doi.org/10.1016/j.engfracmech.2022.108493
Received 27 July 2021; Received in revised form 15 April 2022; Accepted 21 April 2022
Available online 26 April 2022

Nomenclature

Latin

a	Crack length
a_0	Initial crack length
a_{ei}	Equivalent crack ($i = \mathrm{I}, \mathrm{II}$)
b	Mid-plane specimen thickness
B	Specimen thickness
C_i	Specimen compliance ($i = \mathrm{I}, \mathrm{II}$)
E_L	Longitudinal elastic modulus
G_i	Strain energy release rate ($i = \mathrm{I}, \mathrm{II}$)
G_{ic}	Fracture energy under pure mode ($i = \mathrm{I}, \mathrm{II}$)
G_T	Total strain energy release rate
G_LT	Longitudinal tangential plane shear modulus
h	Specimen half height
L	Half distance between supports
P_i	Load for any mode ($i = \mathrm{I}, \mathrm{II}$)
$S(\lambda)$	Normalized stress
w_i	Crack opening displacement ($i = \mathrm{I}, \mathrm{II}$)
w_{ic}	Critical crack opening displacement ($i = \mathrm{I}, \mathrm{II}$)
$\overline{w}_i$	Normalized crack opening displacement ($i = \mathrm{I}, \mathrm{II}$)

Greek

δ_i	Displacement ($i = \mathrm{I}, \mathrm{II}$)
σ_i	Stress ($i = \mathrm{I}, \mathrm{II}$)
$\sigma_{i,\mathrm{u}}$	Ultimate strength ($i = \mathrm{I}, \mathrm{II}$)
$\overline{\sigma}_i$	Normalized stress ($i = \mathrm{I}, \mathrm{II}$)
λ	Dimensionless displacement parameter
θ	Normalized mode mixity

ACRONYMS

CODi	Crack Opening Displacement ($i = \mathrm{I}, \mathrm{II}$)
DCB	Double Cantilever Beam
DIC	Digital Image Correlation
ENF	End-Notched Flexure
FPZ	Fracture Process Zone
MMB	Mixed-Mode Bending

tissue. This test consists of a parallelepipedal specimen with a longitudinal crack with a circular hole drilled at its center and submitted to axial compression loading. Due to the hole presence, tensile and shear stresses arise at the crack tip inducing mixed-mode I + II loading. Aliha et al. [12] proposed the sub-sized short bend beam test, which consists on a three-point bending short beam specimen containing an inclined edge crack. This specimen is particularly appealing in the context of bone considering its small dimensions. Pereira et al., [13] have used the single-leg bending test, which consists on a three-point-bending loading on a beam specimen with a shorter and not loaded arm in the region of the pre-crack, in order to induce mixed-mode I + II loading. In fact, the applied loading induces simultaneous longitudinal shear sliding and opening displacements at the crack tip, thus enabling fracture characterization under mode I + II loading. This test is easy to perform but is limited to a unique mode ratio.

The described tests reveal limitations regarding difficult variation of mode ratio and confinement of fracture process zone ahead of the crack tip with consequent non-self-similar crack growth. With the purpose of overcoming these drawbacks, Pereira et al., [14] proposed a miniaturized version of the mixed-mode bending (MMB) test. This test requires a complex loading system but provides fracture characterization under different mixed-mode ratios by simply changing the lever length of the loading arm.

In this work, the previously conceived MMB testing setup [14] is used to perform mixed-mode fracture analysis of bovine cortical bone tissue. The focus will be the evaluation of the mode I and mode II components of the mixed-mode cohesive laws. A common assumption under mixed-mode I + II loading conditions is that the normal stresses are almost independent of the mode II crack opening displacement ($\mathrm{COD_{II}}$) and vice-versa, i.e., the shear stresses depend weakly on the mode I crack opening displacement ($\mathrm{COD_I}$). As a result, the cohesive laws can be decoupled [15,16], i.e., the total energy release rate, G_T, can be separated into the mode I (G_I) and mode II components (G_II). Other methods lie on the influence of $\mathrm{COD_I}$ on shear stresses and $\mathrm{COD_{II}}$ on normal stresses. In this work, two methods were considered for the experimental identification of cortical bone cohesive laws components under mixed-mode I + II loading conditions, using the MMB test: the uncoupled method [15,16] and the coupled method developed by Högberg [17]. Despite the large scatter of experimental results typical of a natural material like bone, important conclusions about the suitability of both methods were drawn.

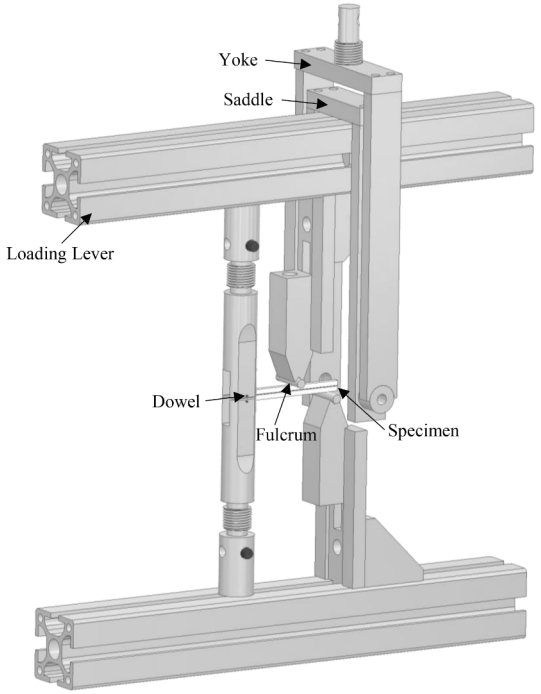

Fig. 1. Schematic representation of the MMB text setup conceived for bone fracture characterization under mixed-mode I + II loading.

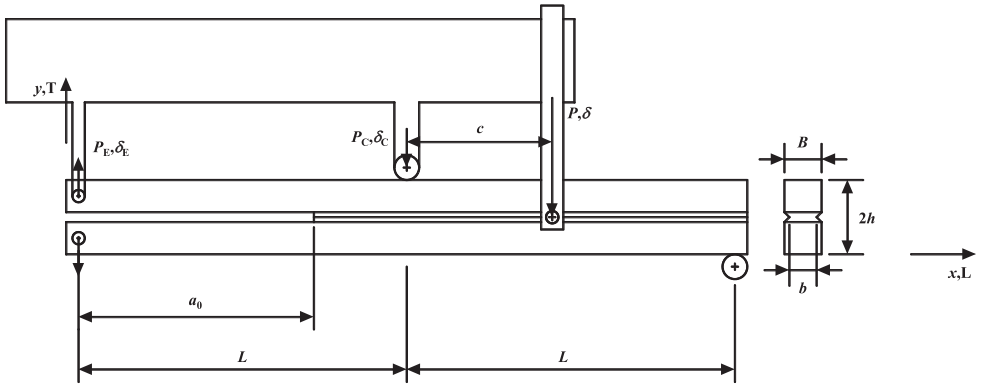

Fig. 2. Schematic representation of the MMB test (L = 30 mm, 2 h = 6.0 mm, b = 2.0 mm, B = 3.0 mm, a_0 = 20 mm).

2. Experimental work

A miniaturized version of the Mixed-Mode Bending (MMB) test setup was conceived [14] for fracture characterization of cortical bone tissue under mixed-mode I + II loading (Fig. 1). The MMB test is a combination of the double cantilever beam (DCB) and the end-notched flexure (ENF) tests using a single lever to apply mixed-mode I + II loadings. The load on the top dowel tends to pull the upper specimen arm resulting on an opening load in mode I similar to that of the DCB test. At the same time, the load at the fulcrum bends the specimen, creating a mode II loading mimicking the one of ENF test. The mixed-mode I + II loading ratio is controlled by the yoke position (Fig. 1). In fact, the relative magnitude of the two resulting loads acting on the specimen can be conveniently changed as a function of the yoke position. A saddle mechanism is used to hold the bearings aligned with the specimen mid-plane and assure the connection between the yoke and the loading lever.

The specimens for the MMB tests were harvested from thirteen fresh bovine femora of young animals within a one-day post-mortem period. They were cut from the interior medial region of the mid-diaphysis and immediately cleaned and wrapped in gauze containing a saline solution and frozen at −20 °C. Subsequently, milling and cutting operations were performed aiming to get samples with a

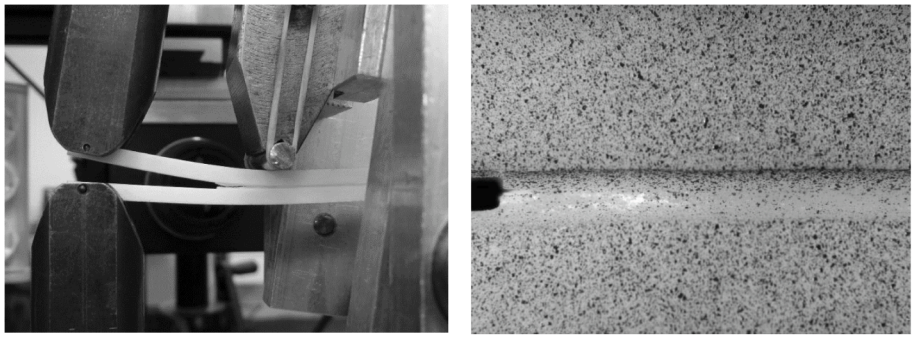

(a) (b)

Fig. 3. a) Back face view of a MMB test; b) Speckle pattern on specimen front face.

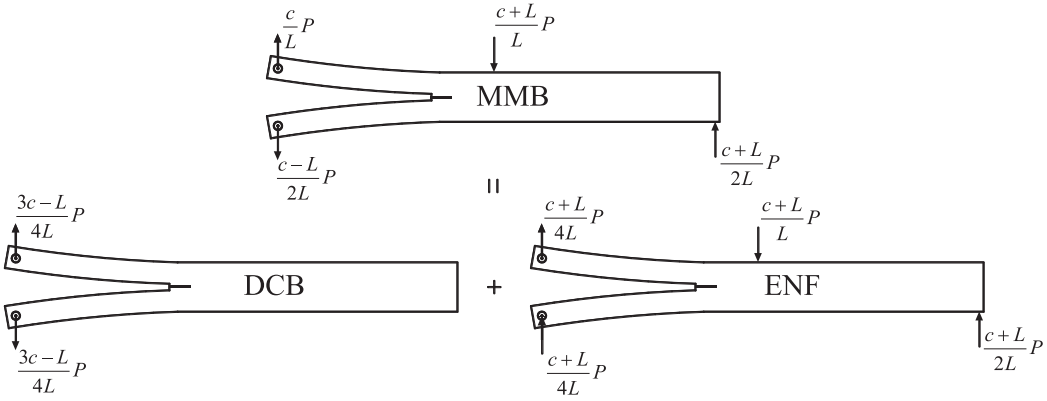

Fig. 4. Superposition loading analysis of the MMB specimen.

width of 3.0 mm, a thickness of 6 mm and a total length of 65 mm. The initial pre-crack was executed in two steps. Firstly, a circular diamond saw with a thickness of 0.3 mm was used to create an initial notch. Secondly, a sharp blade attached to the test machine was employed to induce a natural crack with a small extension of 0.25 mm approximately. The blade was positioned at the notch root and a displacement of 0.25 mm was imposed by the testing machine. Previously, with the purpose of guaranteeing self-similar crack growth at the specimen mid-plane for a given crack extension, two longitudinal grooves with 0.5 mm depth were manufactured using a cutting tool with a V-tip (30°) configuration. Fig. 2 presents a schematic representation of the MMB testing setup with specimen dimensions.

In the MMB test configuration, the G_I/G_{II} mode ratio is defined as [18]:

$$\frac{G_I}{G_{II}} = \frac{4}{3}\left(\frac{3c-L}{c+L}\right)^2, \; c \geqslant \frac{L}{3} \tag{1}$$

The alteration of the mode-mixity is easily performed in the MMB test by changing the lever length of the loading system (distance c in Fig. 2). In fact, it can be seen from Eq. (1) that G_I/G_{II} ratio depends on the distance c, which should be higher than $L/3$ to assure that the mode I loading is strong enough as to open the crack [18]. Three different mode ratios were targeted in this study, to have a good estimation of the bone fracture envelope in the G_I-G_{II} space.

The fracture tests (Fig. 3) were executed using a servo-electrical testing system (MicroTester INSTRON 5848) with constant displacement rate of 0.5 mm/min. A 1 kN load-cell was used and the data acquisition frequency was set equal to 5 Hz. In order to get the evolution of the crack opening displacements during the test, digital image correlation (DIC) (Fig. 3b) analysis was performed with an acquisition frequency of 1 Hz.

3. Data reduction method

The MMB test is a combination of the DCB and ENF tests used for fracture characterization under mode I and II, respectively. Consequently, the MMB loading can be represented by a superposition of a mode I and mode II loadings equivalent to those used in DCB and ENF tests, respectively. This linear combination is schematically represented in Fig. 4. Therefore, the strain energy release

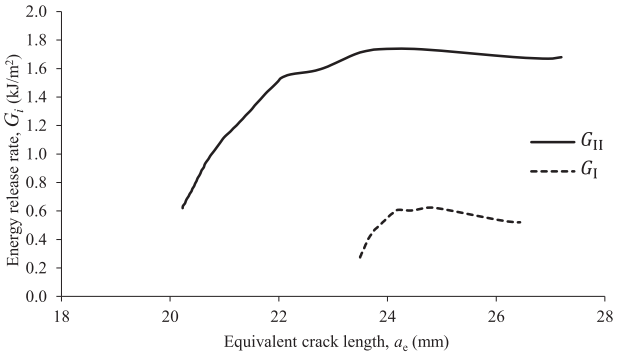

Fig. 5. Example of experimental *R*-curves obtained for $\theta = 47.1^{\circ}$ mode ratio.

rate equations obtained for DCB and ENF tests considering beam theory can be used to obtain the equations for MMB tests. With this aim, the mode I and II loading components can be expressed as (Fig. 4).

$$P_I = \left(\frac{3c - L}{4L}\right)P \tag{2}$$

$$P_{II} = \left(\frac{c + L}{4L}\right)P \tag{3}$$

The relationship between specimen compliance ($C = \delta/P$) and crack length (a) can be established by means of Timoshenko beam theory [4],

$$C_I = \frac{\delta_I}{P_I} = \frac{8a^3}{E_L B h^3} + \frac{12a}{5BhG_{LT}} \tag{4}$$

where δ_I corresponds to the mode I displacement component (δ_E in Fig. 2). Bone is a natural material revealing an important scatter on its longitudinal modulus (E_L), which plays an important role on the measured strain energy release rate. The shear modulus (G_{LT}) has low influence on the results and a typical value can be used. With the purpose of overcome the source of inaccuracy resulting from scatter on E_L, the longitudinal modulus is estimated by an inverse procedure based on fitting the initial specimen stiffness obtained numerically with the experimental one. Eq. (4) can be solved to determine an equivalent crack length (a_{eI}) as a function of the current compliance (C_I) [4]. This procedure avoids the difficult monitoring of crack length during the test and accounts for the presence of a non-negligible fracture process zone (FPZ) in the quasi-brittle materials like cortical bone. The evolution of the strain energy component in mode I can be obtained combining the Irwin-Kies relation.

$$G = \frac{P^2}{2b}\frac{dC}{da} \tag{5}$$

with Eq. (4), yielding,

$$G_I = \frac{12P_I^2}{Bbh}\left(\frac{a_{eI}^2}{h^2 E_L} + \frac{1}{5G_{LT}}\right) \tag{6}$$

A similar procedure can be used for mode II. In this case the equation of the compliance $C_{II} = \delta_{II}/P_{II}$, where $\delta_{II} = \delta_C + \delta_E/4$ (Fig. 2) can be written as [19],

$$C_{II} = \frac{\delta_{II}}{P_{II}} = \frac{3a^3 + 2L^3}{12E_L I} + \frac{3L}{10G_{LT}Bh} \tag{7}$$

where I stands for second moment of area of each specimen arm. The equivalent crack can be obtained from Eq. (7) as,

$$a_{e_{II}} = \left[4E_L I\left(C_{II} - \frac{3L}{10G_{LT}Bh}\right) - \frac{2L^3}{3}\right]^{1/3} \tag{8}$$

The progression of the strain energy component in mode II results from Eqs (5) and (8).

$$G_{II} = \frac{9P_{II}^2 a_{eII}^2}{16BbE_L h^3} \tag{9}$$

The presented methodology allows obtaining the strain energies G_I and G_{II} as function of the equivalent crack length (Fig. 5), i.e., the *Resistance*-curves (*R*-curves). It should be noted that these *R*-curves are obtained using exclusively the P–δ data ensuing from the

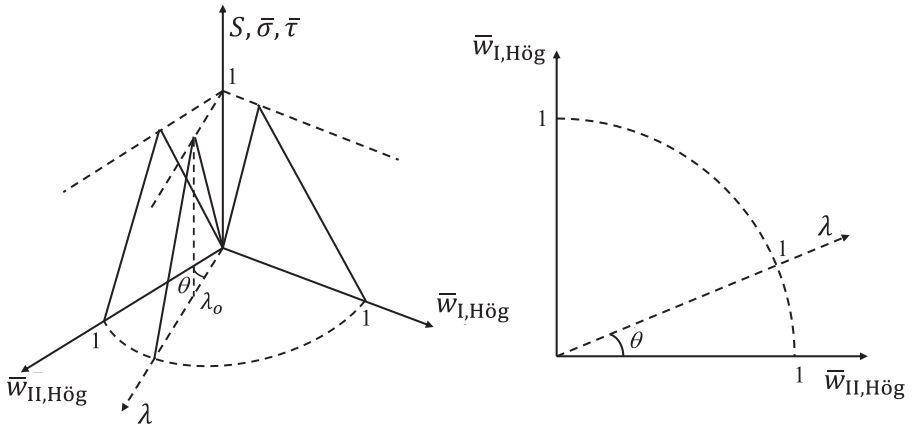

Fig. 6. Graphical presentation of the normalized mixed-mode cohesive law, adapted from Högberg (2006).

MMB test thus being a more appealing procedure, considering the difficulties intrinsic to crack length measurements in this material.

During the fracture tests, the crack tip opening displacement was measured by post-processing DIC displacement fields. To start with, the user needs to define the location of the centroid subset closest to the initial crack tip, typically in the reference speckled image. An algorithm is then applied to estimate the relative displacement among adjacent subsets as an evaluation of both mode I (w_{I}) and mode II (w_{II}) openings during the test [20–21].

4. Cohesive laws determination

Two methods were used to determine the cohesive laws. The uncoupled method proposed in [15,16], assumes that the total energy release rate, G_{T}, can be separated into the mode I (G_{I}) and mode II components (G_{II}),

$$G_{\mathrm{T}} = G_{\mathrm{I}} + G_{\mathrm{II}} \tag{10}$$

Following this strategy, the cohesive laws for each mode component can be directly determined from the differentiation of G_{I} and G_{II} regarding to the corresponding crack opening displacements (w_i),

$$G_i = \int_0^{w_i} \sigma_i(w_i)\, \mathrm{d}w_i \ , \qquad i = \mathrm{I},\ \mathrm{II} \tag{11}$$

A spline function was fitted to the strain energy *versus* crack opening relations ($G_i(w_i)$, i = I, II) to eliminate noise and provide a suitable differentiation of the function.

The coupled method developed by Högberg (2006) [17] was also used to get the components of the cohesive laws under mixed-mode I + II loading. This method implies the introduction of dimensionless parameters. Therefore, the crack opening displacements and tractions (σ_i) were normalized using the material critical values ($\sigma_{i,\mathrm{u}}; w_{\mathrm{ic}}$) obtained in pure modes,

$$\overline{\sigma}_i = \frac{\sigma_i}{\sigma_{i,\mathrm{u}}} \ , \qquad i = \mathrm{I},\ \mathrm{II} \tag{12}$$

$$\overline{w}_i = \frac{w_i}{w_{\mathrm{ic}}} \ , \qquad i = \mathrm{I},\ \mathrm{II} \tag{13}$$

In light of this, the relative displacements and tractions vary in the range of [0, 1]. Högberg (2006) [17] considered the simplest linear cohesive law whose fracture energies in pure modes are given by,

$$G_{\mathrm{ic}} = \frac{1}{2}\sigma_{i,\mathrm{u}} w_{\mathrm{ic}} \ , \qquad i = \mathrm{I},\ \mathrm{II} \tag{14}$$

Normalized fracture energies in mode I and mode II ($\overline{G}_{\mathrm{Ic}} = \overline{G}_{\mathrm{IIc}} = 1/2$) are obtained considering the normalized parameters (Eqs. (12) and (13)). The relative displacements in mode I and mode II are coupled via a dimensionless displacement parameter, λ, defined as,

$$\lambda^2 = \overline{w}_{\mathrm{I}}^2 + \overline{w}_{\mathrm{II}}^2 \tag{15}$$

This parameter uses the normalized crack opening displacements (Eq. (13)) determined using the average critical values obtained under pure mode loading. Högberg also defined the normalized mode mixity (θ), as being the ratio of the dimensionless normal and tangential displacements,

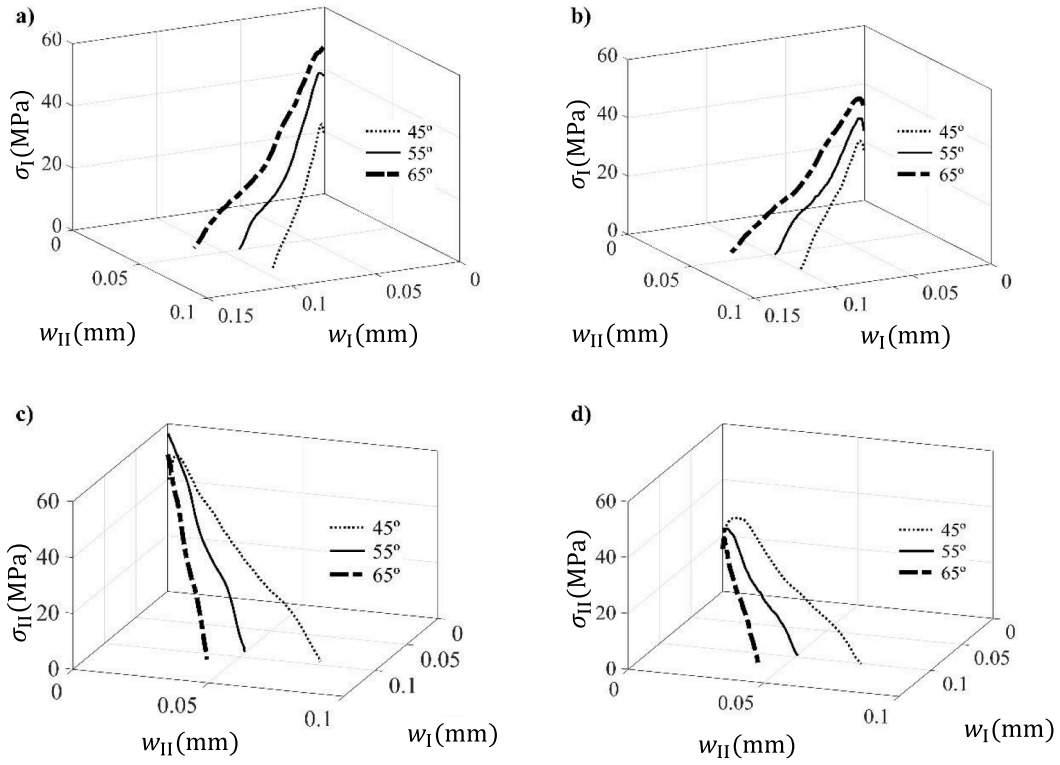

Fig. 7. Averaged cohesive laws as a function of crack opening displacements, for three values of θ: (a) mode I by uncoupled method; (b) mode I by Högberg method; (c) mode II by uncoupled method; (d) mode II by Högberg method.

$$\theta = \arctan\left(\frac{\overline{w}_{\mathrm{I}}}{\overline{w}_{\mathrm{II}}}\right) \tag{16}$$

The pure mode I is given by $\theta = 90^{\circ}$ and the pure mode II by $\theta = 0^{\circ}$. These considerations are graphically presented in Fig. 6, where the traction-separation cohesive relation under mixed-mode loading is established by the normalized stress $S(\lambda)$. For a given θ, S is defined as.

$$S(\lambda) = \begin{cases} \dfrac{\lambda}{\lambda_{\mathrm{o}}} & \text{for} \quad 0 \leqslant \lambda \leqslant \lambda_{\mathrm{o}} \\ \dfrac{1-\lambda}{1-\lambda_{\mathrm{o}}} & \text{for} \quad \lambda_{\mathrm{o}} \leqslant \lambda \leqslant 1 \\ 0 & \text{for} \quad \lambda > 1 \end{cases} \tag{17}$$

being λo the normalized crack opening displacements under mixed-mode at damage onset (Fig. 6). The normalized strain energy release rate is obtained from the area circumscribed by the normalized stress curve. For a given θ,

$$\overline{G}(\lambda) = \int_0^{\lambda} S(\lambda^*)\mathrm{d}\lambda^* \tag{18}$$

The normalized mixed-mode cohesive law ($S = \mathrm{f}(\lambda)$) for each θ can be obtained by differentiation of Eq. (18),

$$S(\lambda) = \frac{d\overline{G}(\lambda)}{d\lambda} \tag{19}$$

where,

$$\overline{G}(\lambda) = \frac{G(\lambda)}{2G_{\mathrm{Tc}}} \tag{20}$$

Considering that the normalized stiffness can be given by the ratio between the normalized stress $S(\lambda)$ and the dimensionless displacement parameter, λ, the normalized tractions in each mode $i = \mathrm{I}, \mathrm{II}$ result,

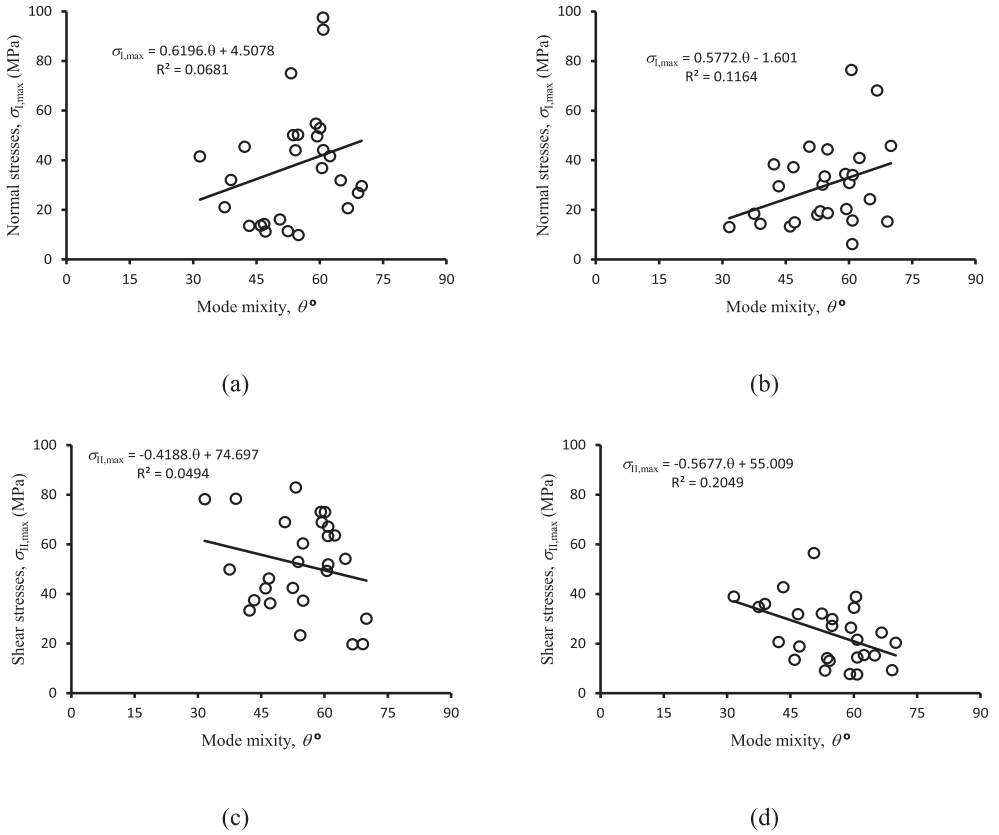

Fig. 8. Evolution of peak tractions ($\sigma_{I,max}$, $\sigma_{II,max}$) as a function of θ: mode I component by (a) uncoupled method; (b) Högberg method; mode II component by (c) uncoupled method; (d) Högberg method.

$$\overline{\sigma}_i = \frac{S(\lambda)}{\lambda}\overline{w}_i \,, \qquad i = \mathrm{I},\ \mathrm{II} \tag{21}$$

which allows the determination of tractions considering Eq. (12),

$$\sigma_i(w_i) = \sigma_{i,\,u}\frac{S(\lambda)}{\lambda}\overline{w}_i \,, \qquad i = \mathrm{I},\ \mathrm{II} \tag{22}$$

5. Results and discussion

The uncoupled and coupled methods described in previous section were applied to estimate the components of the cohesive laws under mixed-mode I + II loading. Three groups of curves have been selected representative of different mode ratios identified by the normalized mode mixity, $\theta = 45^\circ$, 55° and 65°. Fig. 7 (a-d) present 3D plots of the mode I and II components of the average cohesive laws for each θ, obtained by the two methods. Fig. 7a and 7b reveal a consistent trend of the mode I energy component (area circumscribed by each curve) and maximum mode I traction. In fact, both increase with the mode I component, i.e., when θ varies from 45° to 65°. The mode II cohesive law components obtained by the two methods reveal different trends. The mode II energy component and the maximum mode II traction grow with the increase of mode II on mode ratio, i.e., when θ varies from 65° to 45° in the Högberg method (Fig. 7d). This consistent tendency is also observed in the uncoupled method for the mode II energy component, but the peak cohesive traction under mode II loading does not follow the expected tendency. In fact, the $\theta = 55^\circ$ case presents the highest value being the remaining ones similar to each other.

A more detailed analysis regarding the tendencies of the tractions evolution in function of θ were performed for both methods considering all the experimental results (Fig. 8). The first remark addresses the high scatter typical of a natural material, as is the case of cortical bone tissue. In fact, the correlation coefficients are quite low. Nevertheless, the high number of tests performed for each case allows identifying interesting tendencies. First, the normal tractions seem to increase with θ, while the shear tractions reveal an opposite trend. This is a logical result since the pure mode I occurs for θ equal to 90° and the pure mode II for θ equal to 0°.

Linear functions were adjusted to the plots in order to estimate the local strengths under pure modes by extrapolation. Assuming the

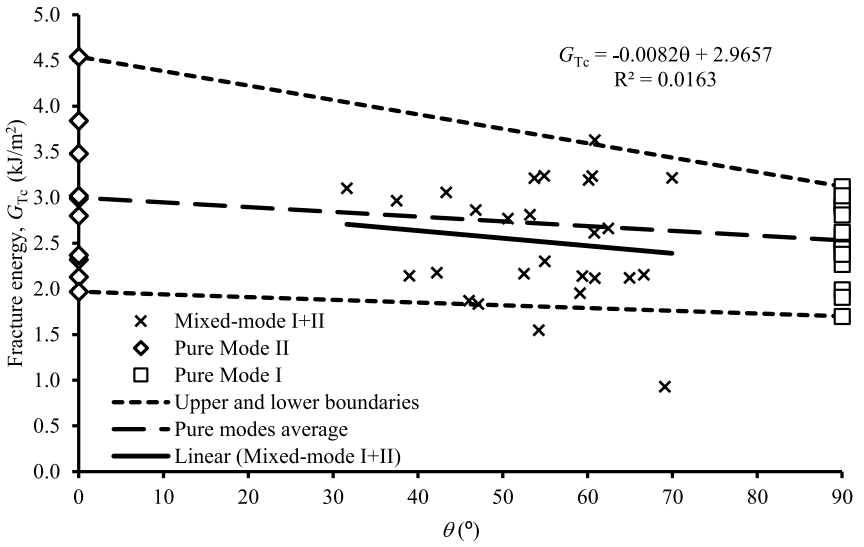

Fig. 9. Fracture energy variation as a function of the normalized mode mixity, θ.

extreme values of $\theta = 0°$ and $\theta = 90°$ in the adjusted functions (Fig. 8), it can be verified that the normal tractions are in the range $4.5 < \sigma_I < 60.3$ MPa for the uncoupled and $-1.6 < \sigma_I < 50.2$ MPa for the Högberg method. Similarly, the limits in the shear tractions are $37.0 < \sigma_{II} < 74.7$ MPa for uncoupled and $3.9 < \sigma_{II} < 55.0$ MPa for the Högberg method. The pure mode local strengths have been determined in a previous work of the research team [6,22]. Using a direct method, values of $\sigma_{I,u} = 49.18$ MPa and $\sigma_{II,u} = 51.01$ MPa and by means of an inverse method $\sigma_{I,u} = 47.25$ MPa and $\sigma_{II,u} = 59.68$ MPa have been achieved. Comparing these values with the ones obtained in this work, it can be concluded that the Högberg method ($\sigma_{I,u} = 50.2$ MPa, $\sigma_{II,u} = 55.0$ MPa) behaves well on the estimation of the local strengths. Moreover, the mode I traction under pure mode II loading ($\sigma_I = -1.6$ MPa) and the mode II traction under pure mode I loading ($\sigma_{II} = 3.9$ MPa) are both close to zero, which reinforces the good behaviour of the model predictions. The uncoupled model predicts $\sigma_{I,u} = 60.3$ MPa and a value of $\sigma_I = 4.5$ MPa for pure mode II loading, which can also be considered a good estimate. However, the same did not occur for the mode II traction components. The predicted value of $\sigma_{II,u} = 37.0$ MPa is lower than expected and a shear traction of $\sigma_{II} = 74.7$ MPa under pure mode I loading is clearly unacceptable. A possible justification for this malfunction of the uncoupled method is probably related with COD measurements. These were performed in points with some distance between them, thus making the uncoupling assumption somewhat inaccurate.

In conclusion, it can be affirmed that even if the linear evolutions of mode I and mode II peak tractions between the pure modes (I and II) presented above could be considered somewhat unsound owing to low correlation coefficients, the results of the Högberg method seem to confirm that these linear trends reveal consistency.

An additional analysis was performed regarding the fracture energy under mixed-mode I + II loading. Fig. 9 plots the experimental results of pure modes ($\theta = 90°$ for pure mode I and $\theta = 0°$ for pure mode II) and the ones of mixed-mode I + II ensuing from this work. Upper and lower boundaries were defined connecting the maximum and minimum values of G_{Ic} and G_{IIc}, respectively. An additional line linking the pure mode (I and II) average values was also included. Two remarks can be drawn. First, the experimental results obtained in this work are circumscribed between the referred boundaries with two exceptions that can be considered outliers. The second and interesting aspect regards the fact that the average trend of the actual results (solid line in Fig. 9) is rather close to the average line referred above. Moreover, extrapolating the solid line in order to estimate the pure mode fracture values gives rise to $G_{Ic} = 2.53$ kJ/m^2 and $G_{IIc} = 3.0$ kJ/m^2, which are in close agreement with the respective average values resulting from DCB and ENF tests, $G_{Ic} = 2.23$ kJ/m^{2}and $G_{IIc} = 2.97$ kJ/m^2. Despite the observed scatter, these findings point to the conclusion that linear energetic fracture criterion describes well the fracture behavior of this set of bovine cortical bone tissue.

6. Conclusions

The mixed-mode bending (MMB) apparatus was adapted to perform mixed-mode fracture tests in bovine cortical bone due to its ability to provide easy alteration of mixed-mode ratio. Three different mode ratios were considered in order to have a suitable description of the mixed-mode fracture behaviour of cortical bone tissue. The main goal was to obtain the mode I and mode II components of the cohesive laws under mixed-mode I + II loading. In this context, a data reduction scheme based on crack equivalent concept was adopted to evaluate the mode I and mode II *R*-curves for each mixed-mode loading, thus avoiding crack length monitoring during the fracture tests. The crack opening and shear displacements were monitored via digital image correlation and correlated with the strain energy release rate components. Two methods were applied to the experimental identification of the cohesive law components under mixed-mode I + II loading: uncoupled method and Högberg's method. Average cohesive laws for each mode ratio were

obtained using the two methods. It was concluded that Högberg's method reveal consistent trends regarding energy components and peak stresses, although the uncoupled method showed some inconsistency on the peak cohesive traction under mode II loading. The tendencies of the tractions evolution in function of the normalized mode mixity were performed for both methods considering all the experimental results. Linear functions were fitted and the pure mode cohesive strengths were estimated by extrapolation. The Högberg's method predicts values in agreement with the ones determined in previous works. The uncoupled method revealed inconsistency on the mode II tractions, which was attributed to inaccuracies inherent to COD measurements. The evolution of fracture energy in function of mode ratio was also analysed. It was observed that the experimental values are bounded by two lines connecting the limiting values of fracture energy and that the average trend of those results agrees with the one resulting from the average values of pure modes, I and II. With some reservations motivated by observed scatter, it was settled that the linear energetic criterion describes well the fracture behaviour of this set of bovine cortical bone tissue.

CRediT authorship contribution statement

Fábio Pereira: Conceptualization, Investigation, Methodology. **José Morais:** Validation. **José Xavier:** Validation. **N. Dourado:** Writing – review & editing, Writing – original draft, Funding acquisition. **M.F.S.F. de Moura:** Writing – original draft, Writing – review & editing, Funding acquisition.

Declaration of Competing Interest

The authors declare that they have no known competing financial interests or personal relationships that could have appeared to influence the work reported in this paper.

Acknowledgements

The first and second author acknowledges the Portuguese Foundation for Science and Technology, under the project UIDB/04033/2020. The third and fifth authors acknowledge the 'Laboratório Associado de Energia, Transportes e Aeronáutica' (LAETA) for the financial support by the project UID/EMS/50022/2019 and the financing of FCT/MCTES through national funds (PIDDAC) and UIDB/00667/2020 (UNIDEMI). The fourth author acknowledges the Portuguese Foundation for Science and Technology, under the project PTDC/EME-SIS/28225/2017.

References

[1] Aliha MRM, Bagherifard S, Akhondi Sh, Mousavi SS, Mousavi A, Parsania H. Fracture and microstructural study of bovine bone under mixed mode I/II loading. Procedia Struct Integrity 2018;13:1488–93.
[2] Koester KJ, Barth HD, Ritchie RO. Effect of aging on the transverse toughness of human cortical bone: Evaluation by R-curves. J Mech Behav Biomed Mater 2011;4(7):1504–13.
[3] Li S, Demirci E, Silberschmidt VV. Variability and anisotropy of mechanical behavior of cortical bone in tension and compression. J Mech Behav Biomed Mater 2013;21:109–20.
[4] Morais JJL, de Moura MFSF, Pereira FAM, Xavier J, Dourado N, Dias MIR, et al. The double cantilever beam test applied to mode I fracture characterization of cortical bone tissue. J Mech Behav Biomed Mater 2010;3(6):446–53.
[5] Norman TL, Nivargikar SV, Burr DB. Resistance to crack growth in human cortical bone is greater in shear than in tension. J Biomech 1996;29(8):1023–31.
[6] Pereira FAM, de Moura MFSF, Dourado N, Morais JJL, Xavier J, Dias MIR. Direct and inverse methods applied to the determination of mode I cohesive law of bovine cortical bone using the DCB test. Int J Solids Struct 2017;128:210–20.
[7] Dourado N, de Moura MFSF, de Morais AB, Pereira AB. Bilinear approximations to the mode II delamination cohesive law using an inverse method. Mech Mater 2012;49:42–50.
[8] Zimmermann EA, Launey ME, Barth HD, Ritchie RO. Mixed-mode fracture of human cortical bone. Biomaterials 2009;30(29):5877–84.
[9] Zimmermann EA, Launey ME, Ritchie RO. The significance of crack-resistance curves to the mixed-mode fracture toughness of human cortical bone. Biomaterials 2010;31(20):5297–305.
[10] George WT, Vashishth D. Susceptibility of aging human bone to mixed-mode fracture increases bone fragility. Bone 2006;38(1):105–11.
[11] Olvera D, Zimmermann EA, Ritchie RO. Mixed-mode toughness of human cortical bone containing a longitudinal crack in far-field compression. Bone 2012;50(1):331–6.
[12] Aliha MRM, Mousavi SS. Sub-sized short bend beam configuration for the study of mixed-mode fracture. Engng Fract Mech 2020;225:106830.
[13] Pereira FAM, de Moura MFSF, Dourado N, Morais JJL, Dias MIR. Bone fracture characterization under mixed-mode I+II loading using the single leg bending test. Biomech Model Mechanobiol 2014;13(6):1331–9.
[14] Pereira FaM, de Moura MFSF, Dourado N, Morais JJL, Silva FGA, Dias MIR. Bone fracture characterization under mixed-mode I plus II loading using the MMB test. Eng Fract Mech, 166, pp. 151–163, Out. 2016, doi: 10.1016/j.engfracmech.2016.08.011.
[15] Mohammed I, Liechti KM. Cohesive zone modeling of crack nucleation at bimaterial corners. J Mech Phys Solids 2000;48(4):735–64.
[16] Yang QD, Thouless MD. Mixed-mode fracture analyses of plastically-deforming adhesive joints. Int J Fract, 110, n. 2, pp. 175–187, Jul. 2001, doi: 10.1023/A:1010869706996.
[17] Högberg JL. Mixed mode cohesive law. Int J Fract 2006;141(3-4):549–59.
[18] Reeder JJC. Mixed-mode bending method for delamination testing. AIAA J, 28(7), 1989, doi: 10.2514/6.1989-1347.
[19] Dourado N, Pereira FAM, de Moura MFSF, Morais JJL, Dias MIR. Bone fracture characterization using the end notched flexure test. Mater Sci Engng, C 2013;33(1):405–10.

[20] Sousa AMR, Xavier J, Morais JJL, Filipe VMJ, Vaz M. Processing discontinuous displacement fields by a spatio-temporal derivative technique. Opt Lasers Engng 2011;49(12):1402–12.
[21] Xavier J, Oliveira M, Monteiro P, Morais JJL, de Moura MFSF. Direct evaluation of cohesive law in mode I of pinus pinaster by digital image correlation. Exp Mech, 54(5), pp. 829–840, Jun. 2014, doi: 10.1007/s11340-013-9838-y.
[22] Pereira FAM, de Moura MFSF, Dourado N, Morais JJL, Xavier J, Dias MIR. Determination of mode II cohesive law of bovine cortical bone using direct and inverse methods. Int J Mech Sci 2018;138-139:448–56.